Received 11 April 2024; accepted 21 April 2024. Date of publication 6 May 2024; date of current version 11 June 2024.
The review of this paper was arranged by Associate Editor Eric Fujiwara.

Digital Object Identifier 10.1109/OJIM.2024.3396843

Pressure Detection With Mach–Zehnder Linearized Tunable Diode-Laser Absorption Spectroscopy

RAOUL-AMADEUS LORBEER, MATTHIAS BITTNER, OLIVER KLIEBISCH, AND PETER MAHNKE

German Aerospace Center (DLR), Institute of Technical Physics, 70569 Stuttgart, Germany

CORRESPONDING AUTHOR: R.-A. LORBEER (e-mail: raoul.lorbeer@dlr.de)

ABSTRACT Tunable diode-laser absorption spectroscopy (TDLAS) sensors have shown to be applicable to, e.g., temperature and pressure measurements in gases. These parameters are indispensable in modern avionics. Even though these systems performed well in laboratory or closed environments, the harsh conditions of avionic flight introduce sources of error. To cope with these challenges, altered variants of the classical direct TDLAS may be taken into consideration. Here, we investigate the differences between an all fiber direct TDLAS and a Mach–Zehnder-based amplitude modulated TDLAS variant. We are able to demonstrate the increased noise immunity of the amplitude modulated system as well as the use of the oxygen A-band for the use as an optical pressure detector.

INDEX TERMS Amplitude modulated tunable diode-laser absorption spectroscopy (TDLAS), flight level, optical air data, oxygen A-band, oxygen spectroscopy, pressure sensor, TDLAS.

I. INTRODUCTION

TUNABLE diode laser absorption spectroscopy (TDLAS) presents a versatile method to preform high-resolution spectroscopy of molecular absorption. The resolved details of the absorbing molecule species allow to deduce properties of the macroscopic environment, such as temperature, pressure, and density. Since optical spectroscopy is a contactless method, it is suitable for measurements under extreme conditions, which otherwise are difficult or even impossible to access [1], [2]. This also applies to the atmospheric conditions around an aircraft which may vary from −55 °C to 50 °C in temperature, from 100 to 1013 hPa in pressure and from extremely dry to oversaturated humidity [3], [4]. Modern pressure sensors covering the atmospheric pressure range are based on piezo-resistive, capacitive, Fabry–Perot interferometer, resonant, variable-reluctance and piezoelectric effects with detailed description in [5], [6], and [7]. Nevertheless, all of these approaches share the necessity to mechanically place a probe in contact to the fluid. Therefore, current air data systems are prone to erroneous behavior or silent failing, e.g., due to mechanical blockage of the pressure port [8] and bound close to the fuselage leading to extensive calibration efforts [9], [10]. This separates TDLAS as a pressure detection method from current implementations and raises the question if and how it will be possible to replace current pressure ports with an external free space TDLAS pressure probe. Practical implementations of TDLAS are nonideal either and suffer from various artifacts. In our context the most important are optical background noise, nonlinear frequency sweeping of the laser source and electromagnetic interference. Especially, weak absorption signals tend to deteriorate due to those effects.

We apply TDLAS in the context of pressure sensing in avionic applications. The experiments presented in this study take the spectroscopic pressure sensing exterior to an aircraft by Buchholz et al. [11] as a reference to potentially improve on. To the knowledge of the authors, Buchholz et al. is the first and only study of a pressure sensing TDLAS air-data system. One design parameter of the system is the laser wavelength and therefore the molecule under investigation, respectively. A molecule homogeneously distributed in the atmosphere up to heights of 12 km is beneficial for the evaluation and reliability of the final system. Furthermore, a wavelength which is easily accessible with current fiber and optoelectronic technologies simplifies the implementation of the system, restricting the wavelength from 400 to 2000 nm. Neutral Ar-atoms and N_2-molecules do not yield significant absorption in this wavelength range. CO_2 shows relevant absorption for wavelength greater than

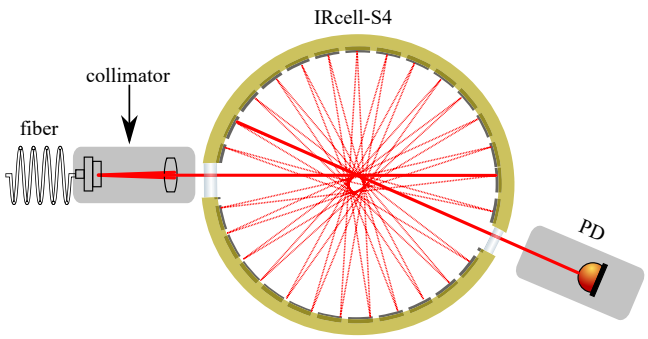

FIGURE 1. Absorption path setup. Spectroscopy light is delivered with a PM fiber, collimated to a free beam and detected with a photo-diode. Multipass cell (IRcell-S4) with reduceable pressure.

2000 nm [12] and H_2O concentration varies by orders of magnitude [3], [11]. Furthermore, H_2O lines mix with all dominant absorption regions with the exception of the O_2 A-band [13]. Therefore, the O_2 molecule with absorption lines around 760 nm in the A-Band [12], [14] was chosen as measuring species. The contactless spectroscopy allows to measure temperature and pressure with minimum disturbance at the measurement volume. In contrast, classical avionic measurement methods either are strongly affected by the boundary layer at the fuselage or require a mechanical probe extending into the measuring volume [9]. The environmental condition of a flight sensor as, e.g., daylight, vibrations, and electromagnetic signals may interfere with the direct (D-)TDLAS method. Multiple approaches to cope with noise in TDLAS applications have been investigated in the past [15]. Furthermore, amplitude modulated (AM-TDLAS) , in the case of temperature measurements, was shown recently to be less prone than D-TDLAS to these kinds of effects [16].

This leads to our approach of developing an all fiber O_2-TDLAS air-data pressure sensor as well as the direct comparison between the passive amplitude modulation technique described in [16] and a standard TDLAS approach in the context of pressure detection. Furthermore we describe a very precise linearizing method to further improve the quality of the Mach–Zehnder (MZ)-based AM-TDLAS technique with continuously software-controlled feedback to the semiconductor laser current. With this method we achieve stabilized sweep-rates of 17.50(1) GHz ms^{-1} at 500 sweeps per second. Furthermore, we were able to show pressure accuracies in the laboratory environment below 4 hPa for D-TDLAS and below 1 hPa for AM-TDLAS. Both systems were studied with active linearization stabilization.

II. MATERIALS AND METHODS

A. SETUP

For the comparison of the two techniques both variants—1) D-TDLAS and 2) AM-TDLAS—are implemented. Both implementations are based on polarization maintaining (PM) fibers. The measurement beam is collimated (Thorlabs F110APC-780) and propagated through a multipass cell (IRcell-S4, IR-Sweep Switzerland) onto a photo-diode (Thorlabs PDA36A2, window removed) as depicted in Fig. 1. The cell is sealed and may be evacuated to investigate pressure depended results.

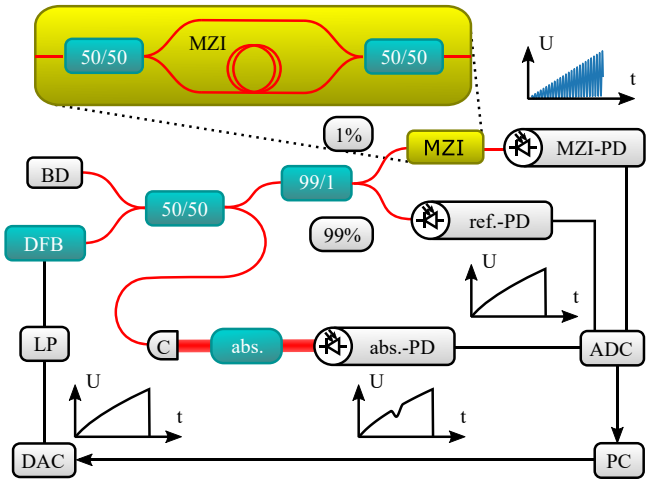

FIGURE 2. Schematic of the direct (D)-TDLAS setup. The DFB-laserdiode (DFB) is directly coupled into a PM fiber. A 50/50 splitter passes radiation to the reference and the measurement fiber. The measurement fiber leads to a fiber collimator (C) and the laser beam is transmitted through the gas-absorption-cell (abs.) onto the absorption photodiode (abs.-PD). The reference radiation passes a 99/1 fiber splitter. 99% of the reference radiation is detected by the reference photodiode (ref.-PD) the remaining 1% passes an all fiber-based MZ interferometer (MZI) and is detected by the MZI photo-diode (MZI-PD). All signals are digitized by an analog to digital converter (ADC), processed and stored by the software on a PC. Furthermore, the MZI-PD data is used to improve the linearity of the DFB sweep by emitting a new control signal via a digital to analog converter (DAC), then passing an analog LP filter and driving the DFB electrical current. Fiber connections are in red, wires in black, and data-flow is indicated by black arrows. Remaining abbreviations are: BD: beam dump, U: voltage, and t: time.

The D-TDLAS implementation is shown in Fig. 2. The system consists of one distributed feedback (DFB)-laser-diode (Eagleyard EYP-DFB-0760-00003-1500-BFY12-0002), which is driven with a periodic sawtooth wave to generate a linear frequency sweep (compare Section II-B). The central wavelength is set by adjusting the temperature of the thermoelectric cooler (TEC) integrated into the laserdiode housing to address the absorption line at 13 142.5767 cm^{-1}. The laser diode has a temperature tuning coefficient of 0.06 nm K^{-1} and a current tuning coefficient of 0.003 nm mA^{-1}. The laser is directly coupled into a PM-fiber, split by a 50/50 splitter, with one half serving as a measurement beam and the second half to characterize the emitted light. 1 % of the characterization light is separated with a 99/1 splitter for wavelength calibration while the remaining 99 % are used as an intensity reference, since the current modulation of the DFB-laser leads to frequency as well as intensity modulations.

The 1 % channel of the splitter is attached to a fiber-based MZ-interferometer with a delay fiber of 2 m in length introduced into one of the interferometer arms. This leads to a full modulation of the transmitted laser radiation at one of the MZ outputs for approximately every 100 MHz of laser-tuning. All signals are captured with amplified photodiodes (Thorlabs PDA36A2) and digitized with an ADC (NI PCIe-6374). The DAC (NI PCIe-6374) signal controlling the DFB-laser current sweep is send through an analog low-pass

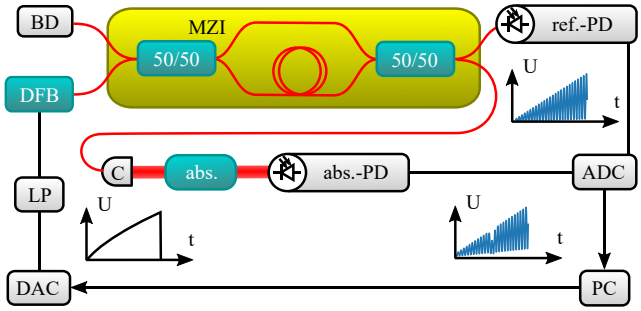

FIGURE 3. Schematic of AM-TDLAS setup. The DFB-laser is coupled into a PM fiber. This radiation is passed through an all fiber MZI. One output of the MZI is directed onto the reference photodiode the other output is collimated and send through the absorption cell onto the absorption photodiode. Both photodiode signals a digitized with an ADC, processed, and stored. The ref.-PD signal is used to reiterate the control voltage for the frequency sweep, via a DAC and an analog LP filter. Fiber connections are in red, wires in black, and data-flow is indicated by black arrows. Abbreviations are: BD: beam dump, DFB: DFB-laserdiode, LP: low-pass filter, DAC: digital analog converter, ADC: analog digital converter, 50/50: 50/50 splitter, C: fiber collimator, abs.: gas-absorption-cell, MZI: fiber MZ interferometer, ref. PD: reference photodiode, abs.-PD: absorption photodiode, PC: personal computer, U: voltage, and t: time.

(LP) filter prior to providing the current control signal to the LD-driver (Koheron CTL200-1-B-200).

The amplitude modulation (AM) of the TDLAS signal was achieved by removing components from the D-TDLAS setup (compare Fig. 3). Here, the laser is coupled directly into the MZ-interferometer. By sweeping the laser-frequency in a linear manner the beat signal will be equivalent to a single frequency amplitude modulated signal source. The second output path of the MZI was used for reference purposes and linearization of the frequency sweep itself, while the original output was utilized as the measurement beam. By demodulation of both signals the absorption can be deduced.

B. LINEARIZATION

In order to achieve a pure single frequency AM-modulation it is essential to generate a perfect linear frequency sweep with the laser source. To achieve linearization the modulation phase $\phi(t)$ of the AM signal $I_{\mathrm{AM}}(t)$

$$I_{\mathrm{AM}}(t) = I_{\mathrm{L}}(t)\cdot\cos(\phi(t) + \phi_0) + I_{\mathrm{back}}(t) \tag{1}$$

has to be measured. Additional factors are the modulation depth $I_L(t)$ and background signal $I_{\mathrm{back}}(t)$. By digitizing the reference signal, the modulation may be averaged over multiple laser sweeps as long as the offset phase ϕ_0 remains a constant with respect to time. The phase is extracted by a variant of the Hilbert-transform which will be referred to as bandwidth limited Hilbert-transform (BW-HT).

It is implemented by a complex (fast) Fourier transform of the time-signal into a frequency signal

$$\tilde{I}_{\mathrm{AM}}(f) = \mathrm{FFT}(I_{\mathrm{AM}}(t)). \tag{2}$$

Initially, the frequency sweep will be broadened due to the nonlinear sweeping responses of the laser diode. A suitably large passband $\mathrm{BP}(f)$ is chosen to pass these modulation frequencies and set all other frequency components to zero

$$\mathrm{BP}(f) = \begin{cases} 1, & 0 < f_{\min} < f < f_{\max} \\ 0, & \text{else.} \end{cases} \tag{3}$$

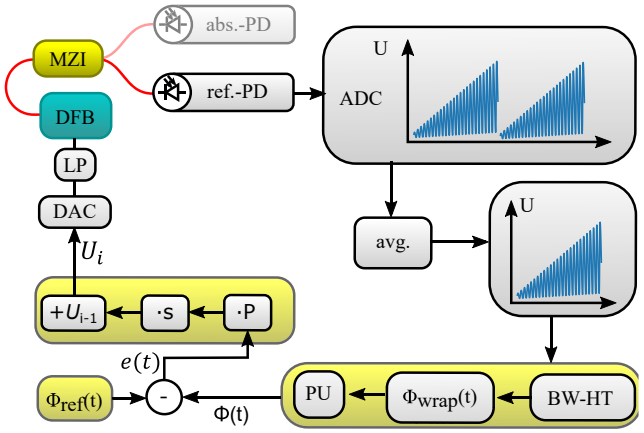

FIGURE 4. Schematic of the linearization loop. The reference photodiode (ref.-PD) detects the modulated signal after the MZ interferometer (MZI). The control loop is implemented digitally starting with an analog to digital converter (ADC) and ending with the digital to analog converter (DAC) and analog LP filter to control the frequency sweep of the DFB laser-diode. The digitized signal is averaged over multiple sweeps, then passed through the BW-HT to generate the wrapped phase ($\phi_{\mathrm{wrap}}(t)$) which than is unwrapped (PU) and subtracted from the desired phase ramp $\phi_{\mathrm{ref}}(t)$. This error-signal $e(t)$ is scaled, added to the previous control voltage sweep and sent to the DAC. Abbreviations: U: voltage, t: time, avg.: averaging of multiple sweeps, BW-HT: Bandwidth limited Hilbert transformation, PU: phase unwrap, P: loop-gain, S: phase to voltage scaler, U_i: voltage in iteration i, LP: electronic low-pass filter, and abs.-PD: absorption detecting photodiode.

The choice of $f_{\min}$ and $f_{\max}$ has to consider the AM-frequency f_{AM} as well as the expected sweep chirp when the algorithm will be initialized. The chirp depends on the specific laser. By observing the initial beat signal after the MZI a bandwidth of $f_{\max} - f_{\min} = 80\,\mathrm{kHz}$ was chosen symmetrically around f_{AM}.

With the assumption that $I_{\mathrm{back}}(t)$ has no significant contributions within the band-pass bandwidth and by applying the inverse FFT a complex time dependent signal is generated, which encodes $\phi(t)$ as

$$S(t) = \mathrm{FFT}^{-1}\left(\mathrm{BP}(f)\tilde{I}_{\mathrm{AM}}(f)\right) = \frac{1}{2} I_L(t)\cdot e^{i(\phi(t)+\phi_0)} \tag{4}$$

$$S(t) = \mathrm{FFT}^{-1}(\mathrm{BP}(f)(\mathrm{FFT}(I_{\mathrm{AM}}(t))) = \frac{1}{2} I_L(t)\cdot e^{i(\phi(t)+\phi_0)}. \tag{5}$$

With the atan2 function applied to $S(t)$

$$\mathrm{wrap}(\phi(t) + \phi_0) = \mathrm{atan2}(\mathrm{Im}(S(t)), \mathrm{Re}(S(t))) \tag{6}$$

the wrapped phase is extracted.

The phase wrapping function is defined as

$$\mathrm{wrap}(\phi) = \mathrm{atan2}(\sin(\phi), \cos(\phi)). \tag{7}$$

After applying a 1-D unwrapping algorithm $\phi(t) + \phi_0$ is retrieved. Ideally $\phi(t)$ resembles a perfectly linear curve with a slope corresponding to the AM frequency $2\pi f_{\mathrm{AM}}$. In this case may be rewritten to

$$I_{\mathrm{AM}}(t) = I_L(t)\cdot\sin(2\pi f_{\mathrm{AM}} t + \phi_0) + I_{\mathrm{back}}(t) \tag{8}$$

where ϕ_0 is an arbitrary start phase.

Fig. 4 shows the implementation of the full linearization loop. The beat signal detected by the reference photodiode is digitized with the ADC and an averaged signal is

generated to reduce susceptibility to noise. A BW-HT is applied to the signal such that $\phi(t)$ may be retrieved. Then, the phase difference $e(t) = \phi_{\mathrm{ref}}(t) - \phi(t)$ to a linear function $\phi_{\mathrm{ref}}(t) = 2\pi f_{\mathrm{ref}} t$ is calculated, where f_{ref} is the desired modulation frequency. The difference signal is scaled by a factor S representing the conversion from phase to control voltage under ideal conditions. Furthermore, a second scaling factor, the loop gain P, is introduced to alter the behavior of the loop. These scaled voltage differences are added to the previous control voltage and converted into an analog signal with a DAC. To reduce stray signals on the analog control input of the laser driver an additional LP-filter of third order is added to the input of the laser driver. To limit the effects on the digital control loop and the shape of the frequency sweep, a bandwidth significantly larger than the actual sweep frequency of 500 Hz and low enough to suppress electrical noise in the relevant electrical bandwidth of the AM-signal had to be chosen. The cut-off frequency (−3 dB) was therefore designed to be 77.5 kHz and measured to be 90 kHz. The phase delay at the cut-off frequency is expected to be approximately 70° which will ultimately contribute to the limitations of the digital control loop. The resulting linearization quality is assessed with three metrics: 1) Δf_{AM}; 2) $\sigma(e(t))$; and 3) $1 - R^2$. To generate a consistent result for these metrics, the signal is cropped to the period which is relevant to the spectroscopy. The first metric is the standard-deviation Δf_{AM} of the beat frequency f_{AM}. To deduce the value, the reference signal from the MZI is converted to its unwrapped phase representation $\phi(t)$ as indicated in Fig. 4. Ideally, this results in a linear phase to time relationship. Since frequency $f_{\mathrm{AM}}(t)$ is given by

$$f_{\mathrm{AM}}(t) = \frac{1}{2\pi}\frac{d\phi(t)}{dt}. \tag{9}$$

Δf_{AM} can be calculated via

$$\Delta f_{\mathrm{AM}} = \sigma\left(f_{\mathrm{AM}}(t)\right) = \sigma\left(\frac{1}{2\pi}\frac{d\phi(t)}{dt}\right) \tag{10}$$

with $\sigma(x)$ returning the standard deviation of x. The second metric is the standard deviation of the phase difference $\sigma(e(t))$. The third metric will be the fraction of variance unexplained (FVU) calculated by $1 - R^2$ with R^2 as the coefficient of determination of a linear fit to $\phi(t)$.

The MZI and absolute frequency of the DFB-laser was calibrated by introducing a thermal sweep to the DFB-LD. This allows to pass multiple absorption lines in the oxygen A-band in a single sweep. By fitting the phase differences of the absorption peaks measured with the MZI to the possible sets of HITRAN listed absorption lines, a high-linear correlation with a FVU of $2 \cdot 10^{-6}$ was achieved. Since the line spacings are not equidistant, the FVU for skipping on absorption line further to larger wavenumbers increases to 0.01 and skipping to lower wavenumbers to 0.004. This allows to verify the absolute calibration of the wavenumber as, e.g., our optical spectrum analyzer reached the limitation of its accuracy. The wavenumbers used for the calibration

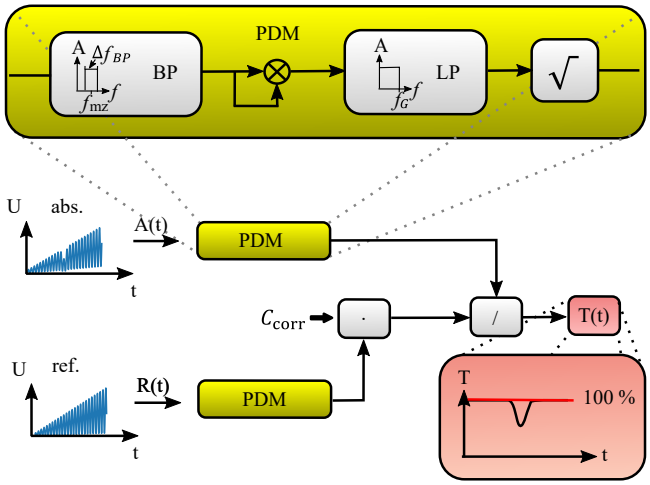

FIGURE 5. PDM and evaluation of AM-signals. The absorption (abs.) signal A(t) as well as the reference (ref.) signal R(t) are demodulated. This is achieved by applying a digital band-pass (BP) filter to the signal, squaring the values elementwise, applying a digital LP filter and taking the square root of the result. By applying a correction factor C_{corr} to the reference signal and a samplewise division (/), the transmission signal T(t) may be extracted. Abbreviations: U: voltage, t: time, BP: digital band pass filter, and LP: digital low-pass filter.

therefore were 13142.5767, 13144.534, 13146.5736, and 13 148.1281 cm^{-1}. The MZI was determined to have a phase to wavenumber ratio of 1920±2 rad/cm^{-1}.

C. DEMODULATION

Demodulation of the AM-signal is achieved by a digital implementation of product demodulation (PDM) [17]. As depicted in Fig. 5 the measurement signals of the absorption as well as the reference channel are demodulated with the same method. A band-pass filter is applied to the signal to reduce information to the frequencies close to the AM-frequency. Subsequently, all values are squared, which leads to a frequency mixing similar to classical AM-demodulation. Afterward, a LP filter removes higher-modulation frequencies such that all relevant frequencies shifted close to the zero-frequency remain. To compensate for scaling errors introduced by the squaring process the square root of the LP signal has to be taken. The resulting information represents the desired absorption and reference signal. For the choice of the filter bandwidths, the expected linewidth has to be considered. In the range from 200 to 1000 hPa a linewidth > 1 GHz is to be expected. At the set sweep rate of 17.5 GHz ms^{-1} this corresponds to approximately > 50 µs or a signal with a bandwidth of < 20 kHz. Since amplitude modulations contribute symmetrically around the carrier frequency the full bandwidth of the band-pass was chosen to be at 40 kHz and the bandwidth of the LP was set to 20 kHz.

D. EVALUATION

The evaluation of the AM- and D-TDLAS signals was performed identically to ensure a straight forward comparison. Due to differences in detector sensitivity and

transmission losses for the different channels the reference signal is multiplied by a correction factor c_{corr}. To achieve comparable absorption lines the digital LP filter applied to the AM-TDLAS signal was applied to the D-TDLAS signal as well.

Thereafter, the absorption signal is divided by the scaled reference signal to determine the transmission signal

$$T(t) = \frac{A(t)}{C_{\text{corr}} R(t)}. \tag{11}$$

As described by the Lambert–Beer law, the extinction ε may be deduced

$$\varepsilon(t) \ = -\ln(T(t)). \tag{12}$$

This extinction can be modeled as a Voigt profile. By fitting a Voigt profile with prior knowledge of the gas composition and the gas temperature, the pressure dependent broadening can be deduced and converted to ambient pressure [11]. In our case the best results were achieved by additionally fitting a third order background polynomial to the edge areas of the detected spectrum and subtracting this artificial background $\text{bg}(t)$ from the measured signal $\epsilon(t) - \text{bg}(t)$. The succeeding Voigt-fit to the full signal preformed significantly better with the reduced background signal. Vice versa the fitted Voigt profile $V(t)$ was removed from the original signal $\epsilon(t) - V(t)$ returning a better reference to fit to the background. These steps were iterated multiple times. Typically, 100 iterations were sufficient to reach a converging result.

In the experiments the fit results were referenced to a piezoresistive pressure sensor (Keller PAA-33X). The pressure sensor is specified to reach an accuracy of 0.5 hPa in the range from 0 to 1 bar with the initial calibration. Using the parameters given in the "high-resolution transmission molecular absorption" (HITRAN) database [12], [18] the pressure was deduced. It became apparent that the deduced pressure values do have a scaling error and an offset, which became more relevant for smaller pressures. The simple assumption of a wrong set temperature underestimating the Gaussian broadening and slightly off values in the HITRAN database could explain this behavior. Unfortunately, the known tolerances to the temperature measurement and the HITRAN database values are not sufficient to explain the observed effect [12], [18].

Plausibility tests to verify the signal properties via multiple lines showed that the absorption strength of the lines support the expected frequencies. This verifies that the laser actually was emitting at 13 142.5767 cm^{-1}. Since the broadening of the absorption line due to pressure broadening is dependent on the distinct line, different absorption lines will have slightly different scaling factors to calculate the pressure from the line width [11]. In contrast to the line strengths the scaling of the slopes and therefore line broadening actually vanished by assuming the neighboring absorption line at 13 144.53 cm^{-1}, which indicates an "off by one" error in the HITRAN absorption line table. The pressure offset most likely is introduced by a broadening of the line-shape introduced by the 20 kHz LP filter applied to the signals. Due to the nature of the AM-TDLAS signal this effect cannot be completely avoided and has to be compensated.

Since the absorption line effectively is convolved with the impulse responses of the applied low- and band-pass filters a first approach is to add the variances of the absorption line σ^2_{Voigt} and the filter impulse response σ^2_{filt} leading to a new total variance σ^2_{TDLAS}. With the standard deviation $\sqrt{\sigma^2}$ as a measure for the line width this leads to

$$\sigma_{\text{TDLAS}} = \sqrt{\sigma^2_{\text{filt}} + \sigma^2_{\text{Voigt}}}. \tag{13}$$

During the fitting procedure, the temperature broadening is already subtracted from the final pressure broadening which, at a given temperature, is proportional to the pressure. Therefore, it is expected to observe a pressure dependency which resembles a hyperbola function

$$p_{\text{TDLAS}} = \sqrt{\text{offset}^2 + (\text{slope} * p_{\text{ref}})^2}. \tag{14}$$

For positive offset and slope this function can readily be inverted to

$$p_{\text{ref}} = \sqrt{(\text{slope} * p_{\text{TDLAS}})^2 - \text{offset}^2}. \tag{15}$$

The offset and slope values used for correction are shown in Table 1.

III. RESULTS

A. LINEARIZATION

The primary parameter in tuning the linearization loop is the loop gain P. The frequency response factor S was calculated from the voltage to current response of the laser driver and the current to frequency detuning rate of the laser diode as stated in the data sheets. Under ideal conditions fastest linearization is expected for $\text{P} = 1$. For $\text{P} \leq 1$ it is expected to require more iterations to achieve linearization, while the susceptibility to oscillations should be reduced. Multiple series assessing the linearization quality for P = [0.2, 0.4, 0.6, 0.8, 1.0] are displayed in Fig. 6. All three metrics Δf_{AM} (top), $\sigma(e(t))$ (left) and $1 - R^2$ (right) indicate that very low levels of remaining error were reached. Occasionally, the iteration of Δf_{AM} and $\sigma(e(t))$ do not converge steadily (Fig. 6 $\text{P} = 0.4$ at iteration 10). Nevertheless, this effect is far less prominent in the FVU and the system operates stable over the whole range of P. As expected, the iterations necessary to reach a steady noise-floor are reduced for larger P. Typically, beat-frequency deviations Δf_{AM} of 100 Hz were reached for beat-frequencies f_{AM} of 170 kHz. This corresponds to a phase error $\sigma(e(t))$ of several mrad or an FVU in the order of 10^{-10}.

B. PRESSURE MEASUREMENT STABILITY

With the successful linearization of the frequency sweep it was possible to directly compare the pressure evaluation of the direct and amplitude modulated TDLAS method with essentially the same system components and an

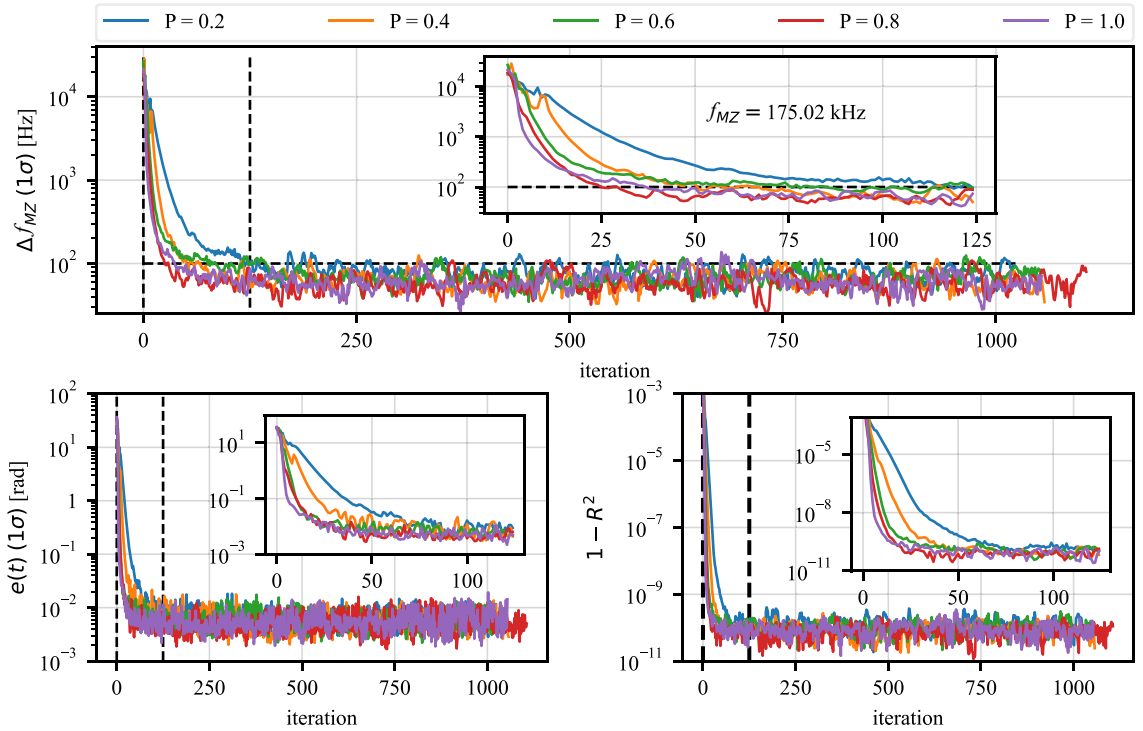

FIGURE 6. Results for linearization loop. Shown are the deviations from an ideally linearized signal for multiple loop-gains (P) plotted against the number of iterations. The metrics plotted are the standard deviation of the frequency error Δf_{AM} (top), the standard deviation of the phase difference $\sigma(e(t))$ (left), and the FVU calculated by $1 - R^2$ with R^2 as the coefficient of determination of a linear fit to $\phi(t)$ (right).

identical modulation of the laser diodes. Fig. 7 shows the overlapping Allan-Deviation for several repetitions of a two minute measurement at constant room pressure with the D-TDLAS system. At short averaging times τ around 10 ms the D-TDLAS system yields an Allan-Deviation well below 1 hPa. Unfortunately, the Allan-Deviation increases for averaging times above 100 ms in all five repetitions and reaches a final level around 1 hPa at averaging times of several seconds. In stark contrast, the AM-TDLAS (Fig. 8) system does lead to a σ_{oadev} of 10 hPa at 10 ms averaging time. Nevertheless, averaging leads to increasing accuracy. At 1 s of averaging, the σ_{oadev} of AM-TDLAS typically falls below 2 hPa while still improving with larger averaging times.

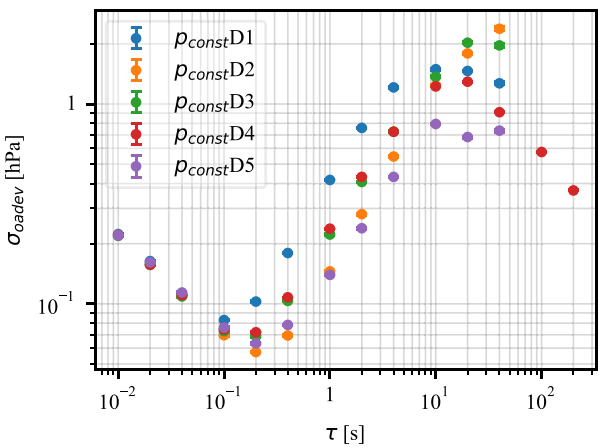

FIGURE 7. Overlapping Allan deviation of multiple runs with the D-TDLAS system. Pressure in the gas cell is steady for several minutes.

C. PRESSURE CORRELATION

Since both methods typically stay below an error of 2 hPa for $\tau \geq 1$ s, the quality of both methods should approach similar results for an averaging time of 1 s. With this 1 s averaging the correlation plots in Fig. 9 (D-TDLAS) and Fig. 10 (AM-TDLAS) were evaluated. To create the varying pressure for both the reference sensor and the TDLAS-systems the optical multipass cell was evacuated until the pressure dropped below 100 hPa. A magnetic valve was attached to a variable leak valve. By controlling the opening time of the magnetic valve and setting the leak valve to a very low-inflow rate, the pressure rose in a controlled, stepwise manner over 500 s. Due to the low rise in pressure, lagging effects in the systems are omitted. The plots show the spectroscopically evaluated pressures against the pressure detected by the reference sensor. Both methods deliver the same pressure evaluations over the total range from 200 to 960 hPa (atmospheric pressure at laboratory location). The signals follow a linear curve and, as expected from the Allan deviations, show small uncorrelated deviations from the ideal linear curve. The hyperbola correction from (15) was applied. The correcting values for D- and AM-TDLAS are given in the corresponding plot figures.

To clarify the achieved linearity, the residuals to an ideal correlation to the reference sensor are plotted underneath the correlation plots. As can be seen in Fig. 9 the residuals

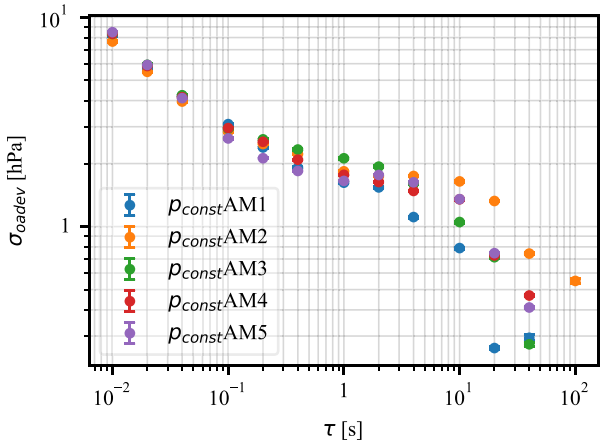

FIGURE 8. Overlapping Allan deviation of multiple runs with the AM-TDLAS system. Pressure in the gas cell is steady for several minutes.

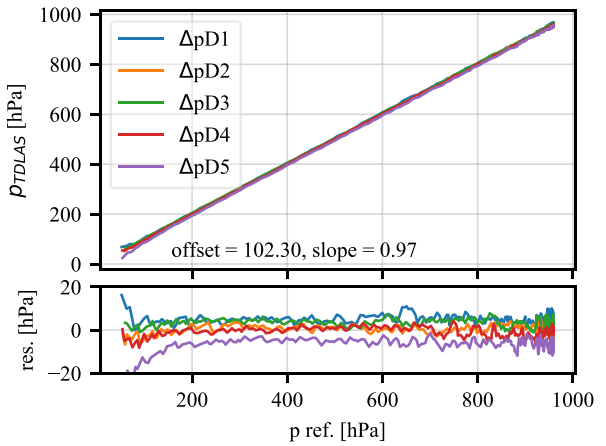

FIGURE 9. Correlation plot of D-TDLAS pressure results plotted against the pressure detected with the reference pressure sensor. The bottom plot shows the residual (res.) to an ideal correlation.

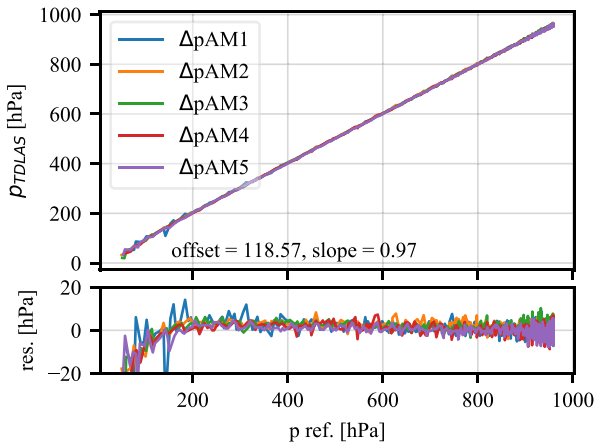

FIGURE 10. Correlation plot of AM-TDLAS pressure results plotted against the pressure detected with the reference pressure sensor. The bottom plot shows the residual (res.) to an ideal correlation.

are quite narrow with a standard deviation between 200 and 960 hPa around 2.1 hPa (compare Table 1). Nevertheless, the repetition of the experiment shows the drift of the values relative to each other over time. Ideally, all residuals should stay on top of each other. As a figure of merit the average deviation from the ideal residual in the range from 200 and 960 hPa has been calculated and is shown in Table 1. It is evident that the five repetitions of the D-TDLAS system yield results in a range of 9.6 hPa with a standard deviation of 3.85 hPa.

TABLE 1. Summary of residual properties for pressure correlation measurements.

Measurement	std. abs [hPa]	avg. abs [hPa]	std. rel	offset [hPa]	slope
Δ pAM1	2.62	-0.48	0.0052	118.57	0.97
Δ pAM2	2.49	-1.14	0.0041	118.57	0.97
Δ pAM3	2.50	-1.35	0.0043	118.57	0.97
Δ pAM4	2.66	0.36	0.0040	118.57	0.97
Δ pAM5	2.63	0.49	0.0037	118.57	0.97
Δ pD1	2.16	4.71	0.0041	102.30	0.97
Δ pD2	2.11	-0.13	0.0030	102.30	0.97
Δ pD3	2.08	-3.08	0.0040	102.30	0.97
Δ pD4	2.01	0.81	0.0026	102.30	0.97
Δ pD5	2.08	6.53	0.0042	102.30	0.97

This behavior was not observed with the AM-TDLAS system, the pressure measurements lie within a range of 1.9 hPa with a standard deviation of 0.84 hPa. The repetitions of the experiment are identical within the range of error. Furthermore, as expected, the standard deviation of the residuals are around 2.5 hPa (compare Table 1) and therefore very close to the standard deviation of the D-TDLAS measurements.

IV. DISCUSSION

This work demonstrates the implementation of an AM-TDLAS system utilizing a highly linearized frequency sweeping laser source in combination with a MZI. Work utilizing a similar setup was recently published by Xu et al. [1], [16], Hou et al. [17], and Xie et al. [19] demonstrating this approach in the context of flame or gas temperature measurements with water vapor. In our work D- and AM-TDLAS were compared utilizing identical components for the deduction of atmospheric pressure with O_2 A-Band spectroscopy. This comparison was made to identify the suitability of the AM-TDLAS implementation for succeeding flight experiments. The relevant pressure for flight experiments ranges from 190 hPa (ICAO standard atmosphere at 12 km) [20] to 1013 hPa (sea level). In our experiments, we were limited to 960 hPa due to the altitude of our laboratory location.

The absorption cross section of O_2 is rather small, resulting in approximately 3 % peak attenuation for every meter of the absorption path. At reduced pressure the line broadening decreases, which compensates the reduction in O_2 density. Nevertheless, at 200 hPa the peak attenuation is reduced to approximately 2 % m^{-1}. Therefore, it is essential that both techniques are very sensitive and precise for the later evaluation. A very interesting aspect of the AM-TDLAS implementation is the generation of the amplitude modulation with the MZI. This allows to generate AM-frequencies

above 100 kHz without an electronic reference. This strongly prevents inducing electric stray signals interfering with the measurement of the pure signal from the photo-diodes. Additionally, this allows to utilize the same components for both setups omitting effects introduced by differing technologies or products. This includes the lasers, fiber-components, photodiodes, gas-chamber, and the ADC/DAC-card.

It must be emphasized that the frequency sweep linearization is performed for both methods. Therefore, the AM-TDLAS is actually compared to a D-TDLAS system with nearly perfect time-frequency correlation. This is not a given property of typical D-TDLAS systems. The data shows that the beat signal of the linearization reached a standard deviation of the residual frequency of 100 Hz given a beat frequency of 170 kHz this corresponds to a frequency-sweep error of $6 \cdot 10^{-4}$. Even though not shown in this article, this precise linearization allows the application of evaluation techniques that rely on an equidistant frequency basis, without additional preprocessing. Especially, algorithms based on matrix multiplication and linear algebra profit from this type of signals. Furthermore, it opens up the possibility of real time evaluation utilizing these algorithms since the data is generated with high-spectral accuracy. In the case of pure linear modulation an even faster method compared to the BW-HT might be the use of a IQ-demodulation. The BW-HT used in this work does create an intuitive phase slope, which corresponds to the frequency sweep of the DFB-laser. In the control loop a given linear phase $\phi_{\mathrm{ref}}(t)$ is subtracted from the deduced phase. This is almost identical to an IQ-demodulation, which can be implemented very efficiently.

PDM was chosen to demodulate the AM-TDLAS signals due to its simple implementation. Comparisons with, e.g., IQ-demodulation schemes did not show any significant differences. This is supported by the recent findings of Hou et al. [17] who demonstrated an analog-electronic implementation of the PDM for utilization in AM-TDLAS spectroscopy. With the technology in place the behavior of both systems was analyzed using Allan-deviations and pressure correlation plots. It became apparent that the D-TDLAS system is strongly subject to random-walk-noise, which was not observed with the AM-TDLAS system over a 2 min time period. This came at the cost of a reduced AM-TDLAS SNR by over an order of magnitude for single sweep pressure fits. Currently, no final explanation for this difference was identified.

To understand the difficulty of deducing the pressure from the line shape one may recall the absolute value of the atmospheric pressure of the Allan-deviations. The pressure at 960 hPa dominates the line broadening. Assuming an accuracy of 1 hPa, this corresponds to an approximate change in the line width by 0.1 %. One explanation could be the fluctuations in the signal background, which can partially have a similar shape as the line profile. These fluctuations are sufficient to alter the apparent line width enough to modify the final result. This background can originate from multiple sources. There are electrical offsets in the mV range, background light from the surrounding lighting conditions or incoherent background radiation emitted by the laser sources themselves, which add time modulated signals to the actual measurement. As soon as these signals change over time, this results in fluctuations of the results as observed for the D-TDLAS system. Starting from this assumption it is logical to transfer the system to an AM variant and move the measurement bandwidth away from these background noise sources. As indicated by the Allan-deviations this approach succeeded. Nevertheless, the pressure-SNR was reduced significantly, beyond the amount expected from the reduced signal strength. Again, there is no conclusive proof for the actual source of this degradation. One explanation could be the introduction of electrical noise sources around 170 kHz which fall into the detection bandwidth of the AM-TDLAS system. Modulations in the target frequency region were observed while refining the electrical design to improve the resilience of the system to such effects. Typical candidates as noise sources in this frequency range are voltage converters, which may vary over time to different degrees. Nevertheless, if certain frequencies are coupled into the signal, the resulting waves may not be phase stable to the sweep rate of the TDLAS system and therefore introduce a fluctuating background signal, which may slide relative to the spectrum at unforeseeable rates. This would alter the short term fit results but average out over longer time periods. Due to the chosen ADC, a switch to significantly higher-AM-frequencies was not possible. Nevertheless, if the source of error is dominated by stray inductance from DC/DC conversions or similar sources, this would help to remove their background effects from the signals. Additionally, more sophisticated background removal approaches, depending on the actual noise sources, could be suitable to generate a better SNR for the AM-TDLAS technique.

Another open question is the deviation in the spectroscopically deduced pressure from the reference.

For the purpose of using the system for pressure detection, a simple hyperbola correction function leads to highly correlated results. We identified a slight deviation from the Voigt profile as the most probable source of error, since for low pressures there appears to be an additional broadening of the line-shape. In our case the LP filter does add additional broadening, which we were able to compensate significantly and thereby generating good correlations in the relevant range without the need of a more complex fit model. This approach also easily adapts to additional broadening as, e.g., visible for the AM-TDLAS correction. Here, the most likely explanation is the added line-width due to the additional band-pass-filter present in the PDM. The same effect is to be expected for more sophisticated absorption line modes from [12]. It still needs to be investigated if these are able to further improve deviations. Concerning the correlation slope of 0.97 our data does lead to contradicting results concerning the effective wavenumber of the measurement. From our data we cannot unambiguously decide, if we measure at $13\,142.5767\,\mathrm{cm}^{-1}$ and there is some error in

our measurement process systematically altering the profile width or we actually measure at 13 144.53 cm^{-1} and there is an error in the absorption strength. A third explanation could be an "off by one" error in the HITRAN data, either introduced by our use of the python HAPI package [21] or actually present in the literature values itself. This effect will be cause for future investigations.

The accuracy of the values given by the HITRAN database or an error in the measurement of the gas temperature are not likely to be of relevance yet. In both cases the given tolerances are far too small to explain the observed deviations.

V. CONCLUSION AND OUTLOOK

We were able to perform a direct comparison between direct and amplitude modulated TDLAS. Furthermore, we were able to demonstrate similar performance of both systems for averaging times of 1 s in a lab environment. In the succeeding project the implementation of a TDLAS pressure sensor onto a research air craft is performed. With these results we are confident to reach a meaningful operating point for both systems such that we plan to investigate both variants in a real flight environment. This will allow to compare the relative robustness of both techniques under real world conditions as, e.g., sunlight or air-plane radio signals.

REFERENCES

[1] L. Xu, G. Hou, Y. Li, S. Qiu, Z. Song, and Z. Cao, "A compact noise-immune TDLAS temperature sensor using intensity modulation," in *Proc. IEEE Int. Instrum. Meas. Technol. Conf. (I2MTC)*, 2020, pp. 1–5.

[2] G. Kim, H. Shim, S. Jung, G. Park, and D. Lee, "Robustness and performance evaluation of TDLAS sensor for scramjet intake," *Aerosp. Sci. Technol.*, vol. 141, Oct. 2023, Art. no. 108561. [Online]. Available: https://www.sciencedirect.com/science/article/pii/S1270963823004583

[3] (Nat. Res. Council., Ottawa, ON, Canada). *The Airliner Cabin Environment and the Health of Passengers and Crew*. (2002). [Online]. Available: https://doi.org/10.17226/10238

[4] *Environmental Engineering Considerations and Laboratory Tests*, ATEC Standard MIL-STD-810H, Jan. 2019.

[5] P. Song et al., "Recent progress of miniature MEMS pressure sensors," *Micromachines*, vol. 11, no. 1, p. 56, 2020. [Online]. Available: https://doi.org/10.3390/mi11010056

[6] J. Fraden, "Pressure sensors," in *Handbook of Modern Sensors: Physics, Designs, and Applications*, Cham, Switzerland: Springer Int. Publ., 2016, pp. 429–451. [Online]. Available: https://doi.org/10.1007/978-3-319-19303-8_11

[7] X. Zhang et al., "Membrane-free fiber-optic Fabry–Perot gas pressure sensor with pa-level resolution," *Opt. Laser Technol.*, vol. 150, Jun. 2022, Art. no. 107940. [Online]. Available: https://doi.org/10.1016/j.optlastec.2022.107940

[8] E. N. F. A. Elmajdub and A. Bharadwaj, "Important pitot static system in aircraft control system," *Amer. J. Eng. Res. (AJER)*, vol. 3, no. 10, pp. 138–144, 2014.

[9] E. A. Haering Jr., "Airdata measurement and calibration: Introduction to flight test engineering," Dryden flight research center, Nat. Aeronaut. Space Admin., Edwards, CA, USA, Rep. NASA-TM-104316, 1995.

[10] J. D. Jurado and C. C. McGehee, "Complete online algorithm for air data system calibration," *J. Aircr.*, vol. 56, no. 2, pp. 517–528, 2019. [Online]. Available: https://doi.org/10.2514/1.C034964

[11] B. Buchholz, A. Afchine, and V. Ebert, "Rapid, optical measurement of the atmospheric pressure on a fast research aircraft using open-path TDLAS," *Atmos. Meas. Techn.*, vol. 7, no. 11, pp. 3653–3666, 2014. [Online]. Available: https://doi.org/10.5194/amt-7-3653-2014

[12] I. Gordon et al., "The HITRAN2020 molecular spectroscopic database," *J. Quant. Spectrosc. Radiat. Transf.*, vol. 277, Jan. 2022, Art. no. 107949. [Online]. Available: https://www.sciencedirect.com/science/article/pii/S0022407321004416

[13] A. Barducci, D. Guzzi, P. Marcoionni, and I. Pippi, "Algorithm for the retrieval of columnar water vapor from hyperspectral remotely sensed data," *Appl. Opt.*, vol. 43, no. 29, pp. 5552–5563, Oct 2004. [Online]. Available: https://opg.optica.org/ao/abstract.cfm?URI=ao-43-29-5552

[14] B. J. Drouin et al., "Multispectrum analysis of the oxygen A-band," *J. Quant. Spectrosc. Radiat. Transf.*, vol. 186, pp. 118–138, Jan. 2017. [Online]. Available: https://www.sciencedirect.com/science/article/pii/S0022407316301108

[15] W. Z. Jingsong Li, B. Yu, and W. Chen, "A review of signal enhancement and noise reduction techniques for tunable diode laser absorption spectroscopy," *Appl. Spectrosc. Rev.*, vol. 49, no. 8, pp. 666–691, 2014. [Online]. Available: https://doi.org/10.1080/05704928.2014.903376

[16] L. Xu, G. Hou, S. Qiu, A. Huang, H. Zhang, and Z. Cao, "Noise immune tdlas temperature measurement through spectrum shifting by using a mach–zehnder interferometer," *IEEE Transactions on Instrumentation and Measurement*, vol. 70, pp. 1–9, 2021.

[17] G. Hou, L. Xu, W. Zhou, A. Huang, and Z. Cao, "A interferometer modulated TDLAS temperature sensor by using coherent demodulation," in *Proc. IEEE Int. Instrum. Meas. Technol. Conf. (I2MTC)*, 2022, pp. 1–5.

[18] V. H. Payne et al., "Absorption coefficient (ABSCO) tables for the orbiting carbon observatories: Version 5.1," *J. Quant. Spectrosc. Radiat. Transf.*, vol. 255, Nov. 2020, Art. no. 107217. [Online]. Available: https://www.sciencedirect.com/science/article/pii/S0022407320302016

[19] H. Xie, L. Xu, Y. Tan, G. Hou, and Z. Cao, "Ultra-low sampled and high precision TDLAS thermometry via artificial neural network," *IEEE Photon. J.*, vol. 13, no. 3, pp. 1–9, Jun. 2021.

[20] *Manual of the ICAO Standard Atmosphere: Extended to 80 Kilometres (262 500 Feet)*, vol. 7488, Int. Civ. Aviat. Org., Montreal, QC, USA, 1993.

[21] R. Kochanov, I. Gordon, L. Rothman, P. Wcisło, C. Hill, and J. Wilzewski, "HITRAN application programming interface (HAPI): A comprehensive approach to working with spectroscopic data," *J. Quant. Spectrosc. Radiat. Transf.*, vol. 177, pp. 15–30, Jul. 2016. [Online]. Available: https://www.sciencedirect.com/science/article/pii/S0022407315302466

RAOUL-AMADEUS LORBEER received the Doctoral degree from the Leibniz Universität Hannover, Hanover, Germany, in 2012.

He is a Physicist specialized of Laser-Optical Systems with Leibniz Universität Hannover. He started his career working on laser scanning microscopy techniques. This includes laser tomography, multi photon microscopy, as well as laser ablative cell sorting and laser micromanipulation. In 2015, he was a Research Scientist with the German Aerospace Center DLR, Cologne, Germany, in the field of laser ablative propulsion to experimentally investigate material processing, laser ablative micro thrusters, and laser ablative space debris removal. Since 2018, his work has been directed at the development and investigation of laser based avionic measurement systems. This includes molecular laser spectroscopy as means to detect atmospheric pressure, as well as the development of suitable and more compact laser- and laser-amplification systems.

MATTHIAS BITTNER received the master's degree in "Modulated tunable diode laser absorption spectroscopy for pressure determination utilizing oxygen molecules" from the Institute of Technical Physics, German Aerospace Center, University of Stuttgart, Stuttgart, Germany, in 2021, under the supervision ofRaoul-Amadeus Lorbeer.

He is a Photonics Engineer of Technical Optics. Early in his career, he gained experience in the development of laser-based prototypes for ophthalmology and electronics design. Later he worked on adaptive optics, disk laser amplifiers, and quality control of camera-based sensors. In 2022, he was with Vario-Optics AG, Heiden, Switzerland, and since then has been an Research and Development Engineer Photonics of Integrated Photonics. He is currently working on on-board optical interconnects between active and passive optical components for high-speed data communication modules and the miniaturization of on-chip optical sensor systems.

OLIVER KLIEBISCH received the Doctoral degree from the University of Konstanz, Konstanz, Germany, in 2017.

He is a Physicist of Laser Physics, Technical Optics and Quantum Information Theory. His first career work was in the field of ultrafast optics specifically high repetition rate offset-locked frequency combs for asynchronous optical sampling (currently known as dual comb sampling). He applied this method to time domain spectroscopy, THz generation and spectroscopy, pulse shaping and precision metrology and frequency locking of THz quantum cascade lasers. In 2017, he was with the Institute of Technical Physics, German Aerospace Center, Stuttgart, Germany, and worked in the field of clear air detection and optical air data sensor technologies. Since 2020, he has been the Team Leader for Optical Air Data. His current research is focused on the airborne application of laser-based remote sensing techniques like lidar and spectroscopy.

Dr. Kliebisch is an expert in Laser Doppler Anemometry and is involved in FPGA-based real-time data processing systems.

PETER MAHNKE received the Diploma degree from the University of Kaiserslautern, Kaiserslautern, Germany, in 2001.

He was with the German Aerospace Center, Stuttgart, Germany (DLR e.V.) in 2001. He worked on injection seeded nonlinear optical sources for air-borne differential absorption lidar systems for methane and water vapor. The scope of work shifted to spectroscopy, airborne laser doppler anemometry, and coherent doppler LIDAR.